Electronic Supplementary Material (ESI) for ChemComm.

Supplementary information

Improving the performance of β-diketonate-based Dy^{III} single-molecule magnets displaying luminescence thermometry

Airton Germano Bispo-Jr,[a,b] Laurence Yeh,[a] Dylan Errulat,[b] Diogo Alves Gálico,[a] Fernando Aparecido Sigoli,[b] and Muralee Murugesu*[b]

Contents

Supplementary note S1 – Some examples of SMMs based on mononuclear Dy^{III} β-diketone complexes and multifunctional Dy^{III} SMMs featuring luminescence thermometry

Table S1. Some examples of single-molecule magnets (SMMs) based on mononuclear Dy^{III} β-diketone complexes with the general [Dy(β-diketone)$_3$(X)] (X = terminal ligand) composition and featuring effective barrier (U_{eff}) larger than 200 K compared to the [Dy(acac)$_3$bpm] complex reported herein. The [Dy(acac)$_3$(X)] complexes where X is a terminal ligand coordinated to the Dy^{III} through chelating nitrogen atoms are highlighted with an asterisk (*). H_{dc} stands for the applied static magnetic field, U_{eff} and τ_0 represent the effective barrier and the pre-exponential factor obtained from the Orbach contribution, C and n are the parameters obtained from the Raman process, τ_{QTM} is the time constant of the QTM contribution, and ΔE stands for the energetic difference between the two low-lying energy Kramers doublets (KD) arising from the Dy^{III} $^6H_{15/2}$ ground level.

Complexes	*Pseudo-symmetry*	H_{dc} / Oe	U_{eff} /K	τ_o / s	n	C / K^{-n} s^{-1}	τ_{QTM} / s	ΔE / cm^{-1}	*ref*
[Dy(acac)$_3$bpm] *	D_{4d}	0	309	$3.2\ 10^{-11}$	3.9	$1.4\ 10^{-3}$	$4.5\ 10^{-3}$	187	#
		1200	345	$6.1\ 10^{-12}$	6.1	$3.1\ 10^{-5}$	-	-	
[Dy(BTFA)$_3$(H$_2$O)$_2$]	D_{2d}	1200	296.50	$6.27\ 10^{-12}$	5.70	$1.95\ 10^{-4}$	-	172.8	1
[Dy(acac)$_3$dmdophen]*	D_{4d}	0	284	$1.1\ 10^{-11}$	5.32	$8.0\ 10^{-3}$	$4.8\ 10^{-4}$	130.5	2
[Dy(TTA)$_3$BPP]	D_{2d}	0	234.2	$7.3\ 10^{-11}$	-	-	$3\ 10^{-3}$	156.6	3
[Dy(ntfa)$_3$(Br$_2$-bpy)]	D_{4d}	1200	216.27	$1.31\ 10^{-10}$	5.56	$1\ 10^{-3}$	-	142.5	4
[Dy(ntfa)$_3$(5,5-(CH$_3$)$_2$-bpy)]	D_{4d}	1200	215.76	$2.60\ 10^{-10}$	5.96	$3\ 10^{-3}$	-	76.1	4
[Dy(acac)$_3$dppz] *	D_{4d}	0	187	$3.1\ 10^{-8}$	-	-	$1.3\ 10^{-2}$	-	5
[Dy(acac)$_3$phendion)] *	D_{4d}	0	178	$4.9\ 10^{-9}$	4.4	$1.3\ 10^{-2}$	2.910^{-3}	115.1	4
[Dy(acac)$_3$dpq] *	D_{4d}	0	136	$1.3\ 10^{-8}$	-	-	$6.3\ 10^{-3}$	-	4
[Dy(acac)$_3$tmphen] *	D_{4d}	1000	130.2	$5.92\ 10^{-9}$	-	-	-	131.15	6
[Dy(acac)$_3$Lz] *	D_{4d}	0	112	$4.38\ 10^{-6}$	4.5	0.019	$1.3\ 10^{-3}$	158.05	7
[Dy(acac)$_3$phen] *	D_{4d}	0	63.84	$5.73\ 10^{-6}$	-	-	-	-	8
[Dy(acac)$_3$dppn] *	D_{4d}	0	37.22	$6.72\ 10^{-7}$	-	-	-	-	9

acac$^-$ = acetylacetonate; bpm = 2,2'-bipyrimidine; tta = thenoyltrifluoroacetone; BTFA = 3-benzoyl-1,1,1-trifluoroacetone; bpy = 2,2'-bipyridine; dppz = Dipyridophenazine; dpq = dipyrido[3,2-*d*:2',3'-*f*]quinoxaline; ntfa = 4,4,4-trifluoro-1-(2-naphthyl)-1,3-butanedione; phen = 1,10-phenanthroline; tmphen = 3,4,7,8-tetramethyl-1,10-phenanthroline; dbpy = 4,4'-dimethyl-2,2'-bipyridyl; BPP = 2,3-bis(2,5-dimethylthiophen-3-yl)pyrazino[2,3-f][1,10]phenanthroline; Lz = 2,4-diamino-6-pyridyl-1,3,5-triazine); dmdophen = 2,2-dimethyl-1,3-dioxolo[4,5-f][1,10] phenanthroline; phendione = 1,10-phenanthroline-5,6-dione; dppn = benzo[*i*]dipyrido-[3, 2-*a*:2',3'-*c*]phenazine)

Solvent molecules in the structures are not represented in the chemical formula.

This work.

Table S2. Examples of multifunctional SMMs based on Dy^{III} displaying luminescence thermometry behaviour, comparing the pseudo symmetry of the Dy^{III} polyhedron and the magnetic properties. The applied static field is indicated by H_{dc}, U_{eff} and τ_0 represent the effective barrier and the pre-exponential factor obtained from the Orbach contribution, C and n are the parameters obtained from the Raman process, and τ_{QTM} is the time constant of the QTM contribution. The temperature (T_m) at which the maximum relative thermal sensitivity (S_m) of the luminescence thermometry is achieved is also displayed.

Complexes	***Pseudo-symmetry***	***H_{dc}* / Oe**	***U_{eff}* /K**	**τ_o / s**	***n***	***C* / K^{-n} s^{-1}**	**τ_{QTM} / s**	***S_m* / % K^{-1}**	***T_m* / K**	***ref***
$[Dy(acac)_3bpm]$	D_{4d}	0	309	$3.2\ 10^{-11}$	3.9	$1.4\ 10^{-3}$	$4.5\ 10^{-3}$	1.51	70	#
		1200	345	$6.1\ 10^{-12}$	6.1	$3.1\ 10^{-5}$	-			
$[Dy(tba)_3phen]$	D_{2d}	0	136	$1.02\ 10^{-9}$	5.97	$2.67\ 10^{-3}$	5 (B1)	1.1	50	[10]
$[Dy(acac)_3(H_2O)_2]$	D_{2d}	0	95	$1.6\ 10^{-9}$	4.9	0.006	$1.01\ 10^{-3}$	5.5##	40	[11]
		1500	131	$2.8\ 10^{-11}$	5.6	$1.15\ 10^{-3}$	-	-		
{DyY}*	D_{2d}	500	90.83	$9.55\ 10^{-15}$	7.41	0.73	0.43	3.5	55	[12]
{DyCo}**	D_{2d}	1000	86.5	$1.05\ 10^{-6}$	-	-	-	1.84	70	[13]
$\{Dy_4\}$***	D_{2d}/D_{4d}	0	39.7	$3.9\ 10^{-6}$	3.1	5	$1.0\ 10^{-3}$	1.6	291	[14]
$[Dy_2(tfaa)_6bpm]$	D_{4d}	0	-	-	6.53	0.0132	$3.65\ 10^{-4}$	1.8	5.4	[15]
		800	33	$1.96\ 10^{-5}$	5.35	0.010	0.326			
$[Dy(acac)_3PyAm]$	D_{2d}	1400	-	-	8.16	2.30	$1.12\ 10^{-3}$	0.76	82	[16]
$[Dy(acac)_3PmAm]$	D_{4d}	0	-	-	6.2	$3.22\ 10^{-4}$	$4.14\ 10^{-2}$	2.04	14	
		1400	-	-	6.37	$1.78\ 10^{-4}$	-			
$\{Dy_4Co_4\}$****	D_{2d}, C_{2v}	2000	-	-	3.58	7.0901	-	2.3	240	[17]

* = {DyY} = $Dy_x^{III}Y_{1-x}^{III}(phen)_2(\mu\text{-}OH)_2(H_2O)_2]\cdot[AuI(SCN)_2]_2\cdot phen\cdot 0.5MeCN\cdot 0.5H_2O$ (x= 0, 0.1, 0.02);

** = {DyCo} = $[DyCo(CN)_6(bpyO_2)_2(H_2O)_3]\cdot 4H_2O$

*** = $\{Dy_4\}$ = $[Dy_4(1,1,4\text{-}H_3Lr)_2(OAc)_6]\cdot CH_3OH$ ($1\cdot CH_3OH$);

**** = $\{Dy_4Co_4\}$ = $\{Dy_4Co_4(CN)_{24}(4\text{-benpyo})_{17}(H_2O)\cdot 7H_2O\}_n$.

Solvent molecules in the structures are not represented in the chemical formula.

$acac^-$ = acetylacetonate; bpm = 2,2'-bipyrimidine; tba^- = thiobenzoate; PyAm = 2-amidinopyridine; PmAm = 2-amidinopyrimidine; tfaa = 1,1,1-Trifluoroacetylacetone; phen = 1,10-phenanthroline; 4-benpyo = 4-benzyloxy-pyridine N-oxide; $bpyO_2$ = 2,2'-bipyridine-N,N'-dioxide; OAc = acetate.

This work;

Under 3.6 T;

Supplementary note S2 - Synthesis and characterization

All reagents and solvents were purchased from AmBeed, Strem Chemicals, Oakwood Chemical, and Thermo Fisher Scientific and used without any further purification. The 2,2'-bipyrimidine (bpm) ligand was prepared as described in the literature.[18] For the [Dy(acac)$_3$bpm] (**1**) synthesis**,** [Dy(acac)$_3$(H$_2$O)$_2$] (627 mg, 1.26 mmol) was added to methanol (30 mL) and the mixture was sonicated (20 min.). The resulting colorless suspension was filtered through celite, and the filtrate was mixed with a clear, 10 mL methanolic solution of 2,2'-bipyrimidine (200 mg, 1.26 mmol). The reaction mixture was then sonicated for 10 minutes and left at 2 °C to slowly evaporate. In two days, colorless blocks of single crystals were observed (81.9 mg, molecular weight = 650.03 g mol^{-1}, 10% yield,) and after seven days, the yield was improved to 40% (327.6 mg). FTIR (cm^{-1}), Fig. S1: 3384.72 (w), 3079.50 (w), 2993.02 (w), 2965.30 (w), 2920.10 (w), 2873.40 (w), 2819.46 (w), 1619.18 (m), 1581.42 (vs), 1571.38 (vs), 1563.69 (vs), 1557.85 (vs), 1518.89 (vs), 1515.41 (vs), 1464.06 (s), 1456.37 (s), 1446.32 (s), 1393.33 (vs), 1386.25 (vs), 1354.04 (s), 1328.83 (s), 1292.43 (m), 1260.30 (vs), 1246.53 (m), 1209.01 (m), 1190.98 (m), 1145.11 (w), 1118.40 (w), 1091.55 (w), 1080.12 (w), 1068.60 (w), 1053.27 (w), 1041.74 (w), 1035.17 (w), 1013.75 (m), 1004.99 (m), 943.09 (w), 919.57 (m), 883.38 (w), 829.20 (m), 766.07 (s), 759.61 (s), 686.07 (m), 650.56 (s), 635.96 (m), 530.27 (w). Elemental analysis (CHN) of [Dy(acac)$_3$bpm]·CH$_3$OH: C_{nom} = 44.34; H_{nom} = 4.80; N_{nom} = 8.61; C_{exp} = 44.40; H_{exp} = 4.15; N_{exp} = 8.73. Finally, the experimental powder X-ray diffraction (PXRD) pattern obtained for the ground crystals matches the simulated powder pattern obtained from the single-crystal X-ray diffraction data (SC-XRD) indicating that the crystallinity of the sample is robust after grinding with minimal solvent loss, Fig. S2.

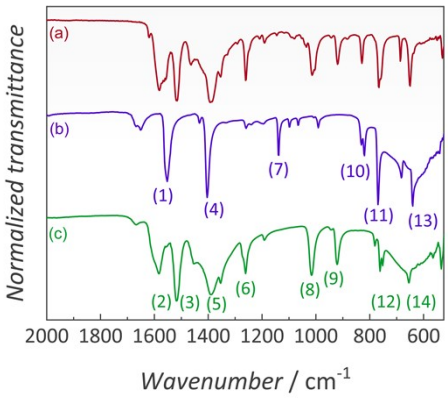

(1)	ν(C=N)+ν(C=C)
(2)	ν(C=O)
(3)	ν(C-O)+(C-H)
(4)	ν_{ring}
(5)	δ(CH$_3$)
(6)	δ(C-H)
(7)	ν(β-CH)
(8)	γ(CH$_3$)
(9)	ν(C-CH$_3$)
(10)	ν(γ-CH)
(11)	ν(γ-CH)
(12)	δ(C-H)
(13)	Ring bending
(14)	ν(L-O) + ν(C-CH$_3$)

Fig. S1. (Left) FTIR spectra of (a) [Dy(acac)$_3$bpm] (**1**), (b) bpm, and (c) [Dy(acac)$_3$(H$_2$O)$_2$]. (Right) bpm (in purple) and acac$^-$ (in green) vibrational mode assignments.

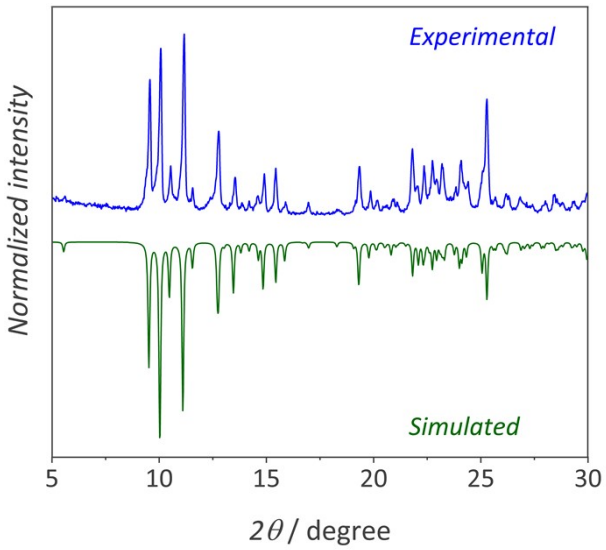

Fig. S2. Powder XRD of ground crystals of [Dy(acac)$_3$bpm] (**1**) compared to the simulated patter determined from the SC-XRD.

Characterization apparatus

Single-crystal X-ray diffraction (SC-XRD). A crystal of **1** suitable for single-crystal X-ray diffraction (SC-XRD) analysis was covered in Parabar 10312 oil and mounted on a 200-µm MiTeGen MicroLoop. Full data was collected on a Bruker AXS SMART equipped with an APEX-II CCD single-crystal diffractometer using graphite-monochromated Mo Kα radiation (λ = 0.71073 Å) at 273 K. Absorption correction was applied by using a multiscan of the SADABS program (v. 2016/2). The raw data collection and processing were performed using the Bruker APEX II software. Using the Olex2 software,[19] the structure was solved using the SHELXT program[20] and refined by the full-matrix least-squares methods on F^2 with the SHELXL-2018/3 program.[21] All non-hydrogen atoms were generated with direct methods and refined with anisotropic thermal parameters while hydrogen atom positions were calculated based on the geometry of their respective atoms.

Powder X-ray diffraction (PXRD). PXRD pattern was obtained in a Rigaku Ultima IV diffractometer using Cu K_α filtered radiation (λ = 1.5401 Å) and one diffracted beam monochromator, at 298 K.

Fourier-transform infrared (FTIR). FTIR spectra were recorded with a Thermo Nicolet 6700 FTIR spectrometer using the attenuated total reflection mode and a transmission window of 4000 to 525 cm^{-1}.

Elemental analysis. C, H, N, elementary analysis was measured in a model varioELcube manufactured by Elementar, Germany.

Photoluminescence. All the photoluminescence data were obtained for the ground crystals using a Quanta Master 8075-21 Spectrofluorometer (Horiba) and a red-extended detector (Hamamatsu R13456 red extended PMT) for the visible spectral region. An ozone-free PowerArc energy 75 W xenon lamp was used as the excitation source. The emission spectra were corrected according to the optical system of the emission

monochromator and the photomultiplier response while the excitation spectrum was corrected in real time according to the lamp intensity and the optical system of the excitation monochromator using a silicon diode as a reference.

Temperature-dependent luminescence. Excitation and emission spectra from 10 K to 270 K were measured in the previously mentioned Quanta Master. To control the temperature, a Janis cryostat (CCS-100/204N model) with an Acme Electric compressor (T181059 model) and a Lake Shore temperature controller (model 335) were used.

Magnetism. DC and AC measurements were performed using a Quantum Design MPMS3 with 22.3 mg of the crystalline sample, which was restrained with silicon grease and wrapped in a polyethylene membrane. The magnetization data were collected at 100 K to confirm the absence of ferromagnetic impurities. Diamagnetic corrections were applied for the sample holder, and the inherent diamagnetism of the sample was estimated with the use of Pascals constants. In order to extend the probed temperature range, AC susceptibility between 1000 Hz – 10 000 Hz was measured on the same sample using a Quantum D Design Physical Property Measurement System (Dynacool-14T) equipped with a vibrating sample magnetometer (VSM).

Supplementary note S3 - Crystallographic data

Table S3. Crystallographic data of [Dy(acac)$_3$bpm] (**1**).

	[Dy(acac)$_3$bpm]·CH$_3$OH
CCDC deposition number	2258317
Empirical formula	$C_{24}H_{31}DyN_4O_7$
Molecular weight, g mol^{-1}	650.03
Temperature, K	273 K
Wavelength, Å	0.71073
Crystal system	Triclinic
Space group	$P\bar{1}$
a, Å	9.2135(4)
b, Å	9.3766(5)
c, Å	16.6513(8)
α, °	94.788(2)
β, °	105.748(2)
γ, °	94.997(2)
Volume	1370.64
No. of formula units/unit cell, Z	2
Density (*ρ*), g cm^{-3} calc'd.	1.575
Absorption coefficient (μ) mm^{-1}	2.773
F(0 0 0)	650
Crystal size, mm^3	0.22 x 0.193 x 0.135
Minimum and maximum transmittance	0.704, 0.746
Theta range, °	1.279 - 27.999
Index ranges (h k l)	(12 12 21)
No. of reflections measured	6622
No. of independent reflections	5887
R(int)	0.0386
Completeness, %	1.000
Data / restraints / parameters	6622 / 1 / 335
R1, wR^2 (I > 2 σ (I))[a]	0.0502, 0.0481
R1, wR^2 (all data)	0.0230, 0.0289
Goodness of fit on F^2	1.056
Largest differential peak and hole, e$^-$/Å^3	0.359; -0.442

[a] $R = R_1 = \sum \frac{||F_0| - |F_c||}{\sum |F_0|}$

$wR_2 = \left\{\sum \left[w(F_0^2 - F_c^2)^2\right] / \sum \left[w(F_0)^2\right]\right\}^{1/2}$

Where $w = 1/\left[\sigma\left(F_0^2\right) + (ap)^2 + bp\right]$

$p = [max(F_0^2, 0)] + 2F_c^2]/3$

$R_w = [w(|F_0| - |F_c|)^2 / w|F_0|^2]^{1/2}$

Where $w = 1/\sigma^2(|F_0|)$

Table S4. Selected bond distances of the DyO_6N_2 coordination polyhedron in [Dy(acac)$_3$bpm] (**1**) compared to the congeners [Dy(acac)$_3$dmdophen],[2] [Dy(acac)$_3$dppz][5], [Dy(acac)$_3$phendione],[2] [Dy(acac)$_3$tmphen][6], [Dy(acac)$_3$Lz],[7] [Dy(acac)$_3$phen],[8] and [Dy(acac)$_3$dppn][9] reported in the literature. These complexes were chosen for comparison because they are Dy^{III}-based complexes coordinated to three $acac^-$ ligands and a neutral bidentate terminal ligand forming two Dy-N bonds. The bond distances were calculated based on the CIF file reported in the CCDC database.

	[Dy(acac)$_3$bpm]	[Dy(acac)$_3$dmdophen]	[Dy(acac)$_3$dppz]	[Dy(acac)$_3$phendione]
CCDC code	2258317	2211014	806774	2211015
Dy-O1 / Å	2.3274(16)	2.3195(16)	2.3153(68)	2.3061(135)
Dy-O2 / Å	2.3360(19)	2.3194(22)	2.3127(68)	2.3250(118)
Dy-O3 / Å	2.3116(19)	2.2983(19)	2.2999(61)	2.3329(127)
Dy-O4 / Å	2.3138(18)	2.2829(20)	2. 3279(71)	2.4099(150)
Dy-O5 / Å	2.3081(20)	2.3404(18)	2.3708(66)	2.3190(146)
Dy-O6 / Å	2.3196(16)	2.3451(22)	2.3122(71)	2.2954(113)
Dy-N1 / Å	2.6211(20)	2.6032(19)	2.5992(63)	2.5946(131)
Dy-N3 (or N2) / Å	2.5842(20)	2.6317(19)	2.5860(73)	2.6015(140)
	[Dy(acac)$_3$tmphen]	**[Dy(acac)$_3$Lz]**	**[Dy(acac)$_3$phen]**	**[Dy(acac)$_3$dppn]**
CCDC code	965722	1513751	801063	1007462
Dy-O1 / Å	2.3460(22)	2.3211(34)	2.321(3)	2.354(3)
Dy-O2 / Å	2.3161(25)	2.3464(29)	2.309(3)	2.305(3)
Dy-O3 / Å	2.3677(17)	2.3119(34)	2.318(3)	2.314(3)
Dy-O4 / Å	2.3200(25)	2.3282(34)	2.335(3)	2.327(3)
Dy-O5 / Å	2.3092(17)	2.3023(35)	2.331(3)	2.347(3)
Dy-O6 / Å	2.3441(19)	2.3218(4)	2.324(3)	2.321(3)
Dy-N1 / Å	2.5696(25)	2.6292(41)	2.558(3)	2.561(4)
Dy-N3 (or N2) / Å	2.5637(18)	2.5646(35)	2.589(3)	2.604(4)

Table S5. Shape analysis of [Dy(acac)$_3$bpm] (**1**) using SHAPE 2.1.[22] Values in the table are the continuous shape measures (CShM, dimensionless) for each idealized geometry.

Idealized geometry	Short name	Point group	CShM
Square antiprism	SAPR-8	D_{4d}	0.893
Triangular dodecahedron	TDD-8	D_{2d}	1.557
Biaugmented trigonal prism	BTPR-8	C_{2v}	2.152
Biaugmented trigonal prism J50	JBTPR-8	C_{2v}	2.801
Snub diphenoid J84	JSD-8	D_{2d}	4.752
Cube	CU-8	*Oh*	8.468
Triakis tetrahedron	TT-8	*Td*	9.311
Hexagonal bipyramid	HBPY-8	D_{6h}	15.227
Johnson gyrobifastigium J26	JGBF-8	D_{2d}	16.579
Heptagonal pyramid	HPY-8	C_{7v}	22.189
Elongated trigonal bipyramid	ETBPY-8	D_{3h}	24.505
Johnson elongated triangular bipyramid J14	JETBPY-8	D_{3h}	28.696
Octagon	OP-8	D_{8h}	31.378

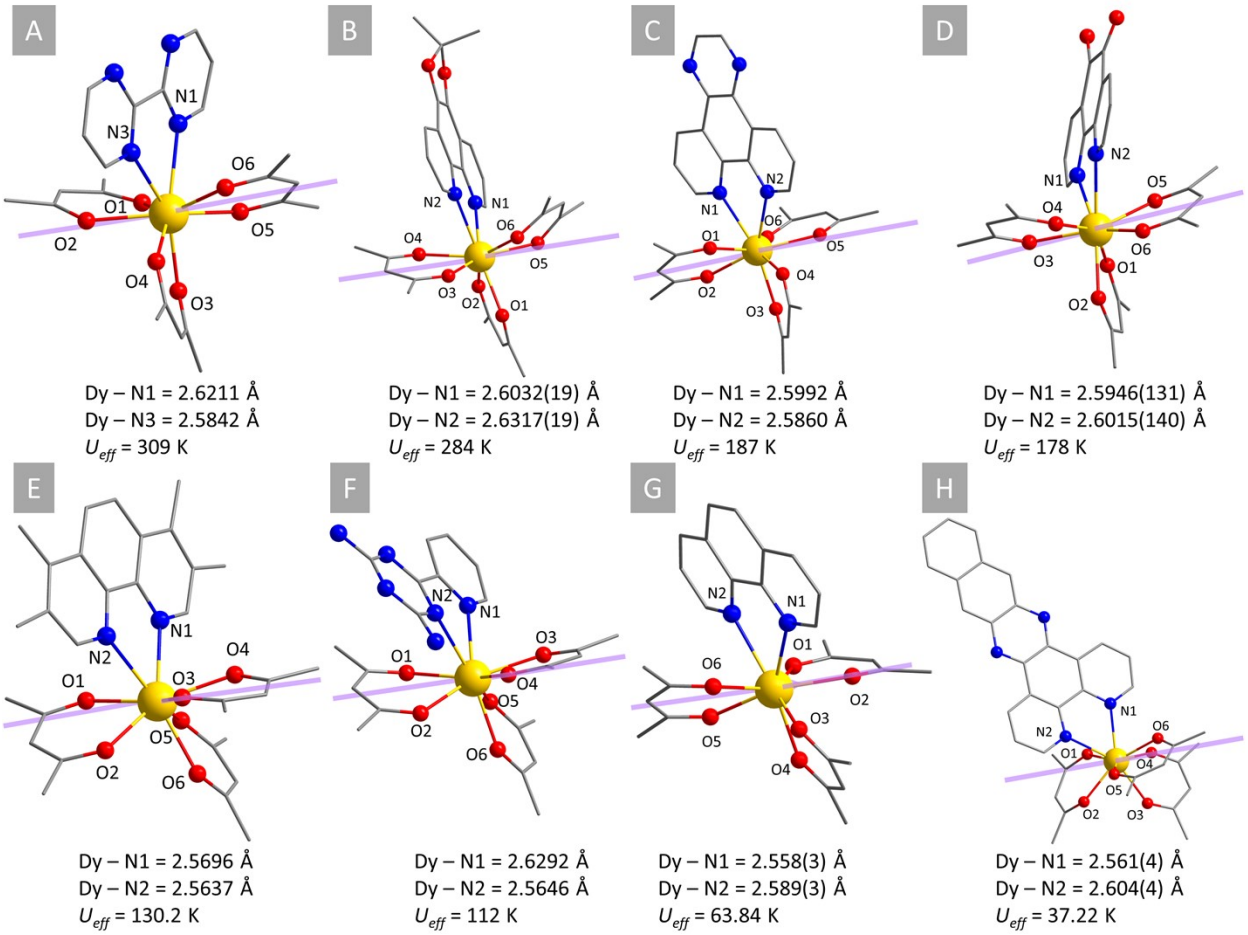

Fig. S3. Molecular structure of (a) [Dy(acac)$_3$bpm] (**1**) compared to congener (b) [Dy(acac)$_3$dmdophen],[2] (c) [Dy(acac)$_3$dppz][5], (d) [Dy(acac)$_3$phendione],[2] (e) [Dy(acac)$_3$tmphen][6], (f) [Dy(acac)$_3$Lz][7], (g) [Dy(acac)$_3$phen],[8] and (h) [Dy(acac)$_3$dppn][9] C = light grey, O = red, N = blue, Dy = yellow. The pink arrow represents the main magnetic axis calculated using the Magellan package[23] for the complexes. The atomic coordinates of the structures reported in the literature were obtained from the CIF files found in the CCDC database (Table S4).

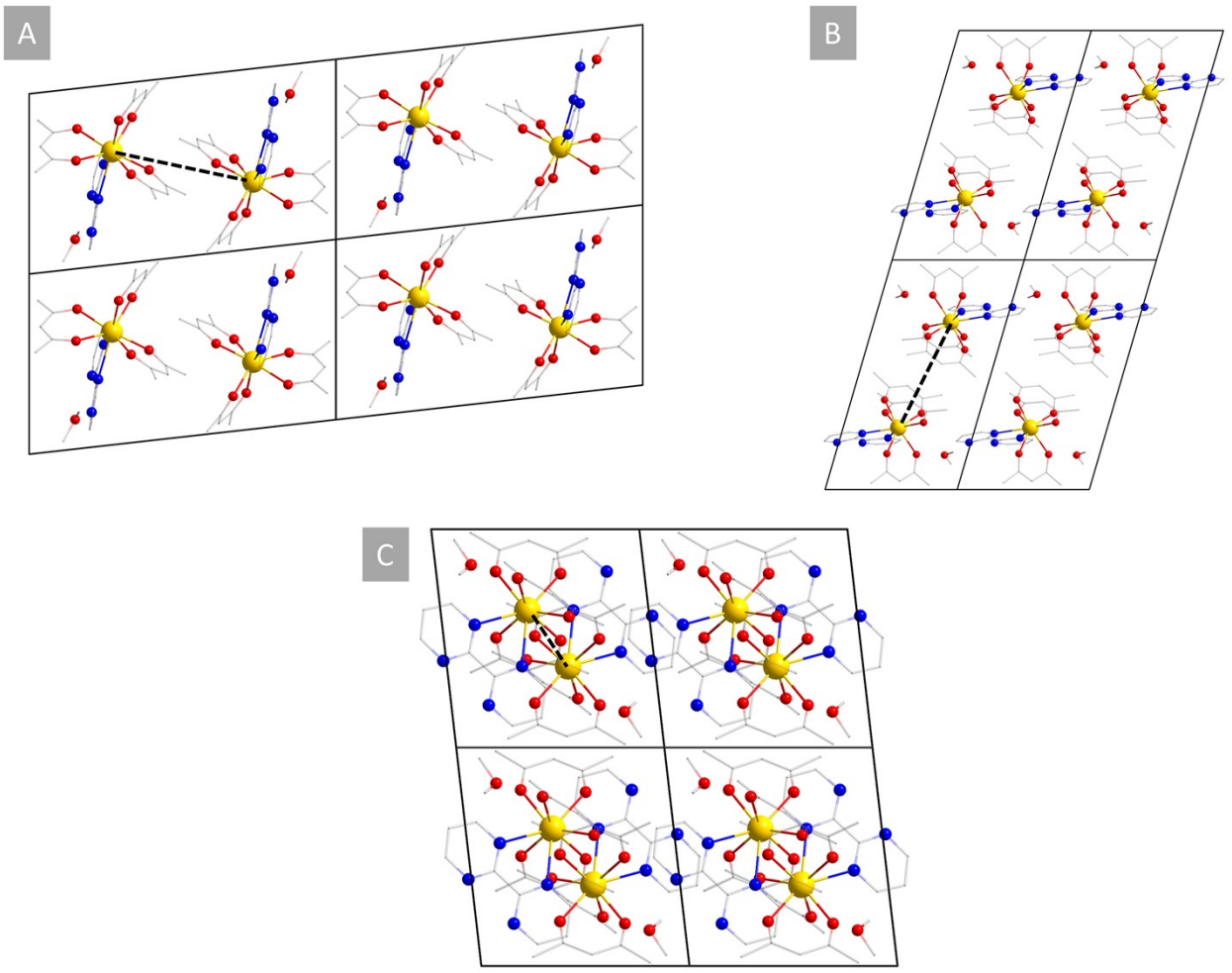

Fig. S4. View of the packing arrangement along the crystallographic (a) *a*, (b) *b*, and (c) c-axis in [Dy(acac)$_3$bpm]·MeOH. Black dashed lines represent the shortest Dy · · · Dy intermolecular distance - 8.4139(6) Å.

Supplementary note S4 - Additional luminescence data

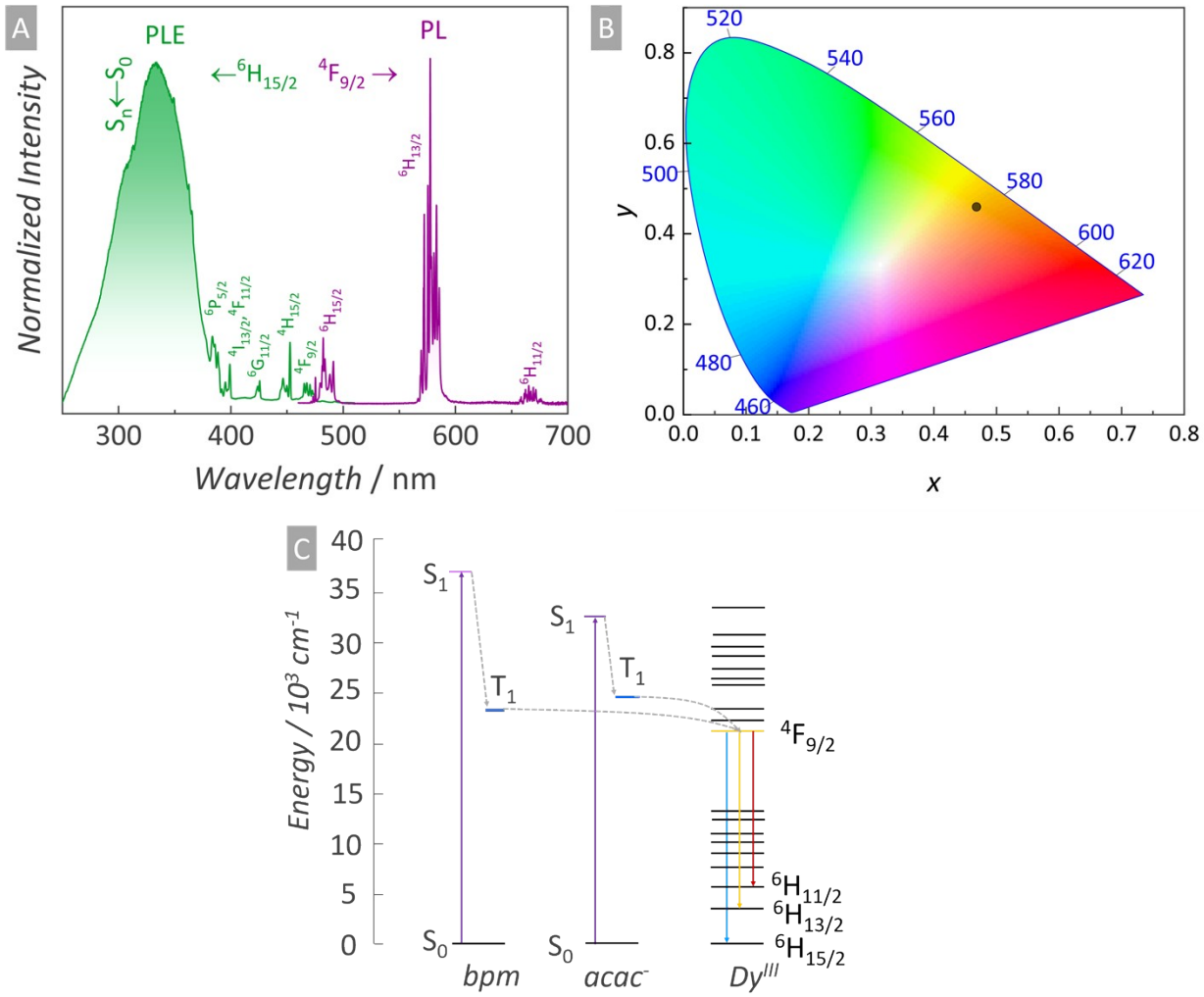

Fig. S5. (a) Excitation (PLE, λ_{em} = 575 nm) and emission (PL, λ_{exc} = 330 nm) spectra measured at 9 K of the [Dy(acac)$_3$bpm] (**1**) as a microcrystalline sample. Assignment of each Dy^{III} *f-f* electronic transition as well as ligand-centered $S_n \leftarrow S_0$ transitions are displayed in the figure. (b) 1931 *Commission internationale de l'éclairage* (CIE) colour coordinate diagram calculated from the emission spectrum of [Dy(acac)$_3$bpm]. (c) Partial energy diagram representing the singlet (S) and triplet (T) energy levels centered on the bpm and acac$^-$ ligands as well as $^{2S+1}L_J$ levels of Dy^{III} (energy transfer from the ligand S_1 levels to the Dy^{III} excited levels may also take place). In the excitation spectrum (Fig. S5a), a broad excitation band is noticed within the 250 – 390 nm spectral range, assigned to $S_n \leftarrow S_0$ electronic transitions of acac$^-$ as well as bpm. Instead, sharp excitation bands lying in the spectral region of 380 – 490 nm come from Dy^{III} *f-f* electronic transitions, arising from the $^6H_{15/2}$ ground level. Upon ligand excitation at 330 nm (Fig S5a), the typical Dy^{III} emission coming from the $^4F_{9/2} \rightarrow {}^6H_{15/2,13/2,11/2}$ transitions are observed, rendering a yellowish-orange emission (Fig S5b) due to ET from acac$^-$ and bpm to Dy^{III} (Fig. S5c).

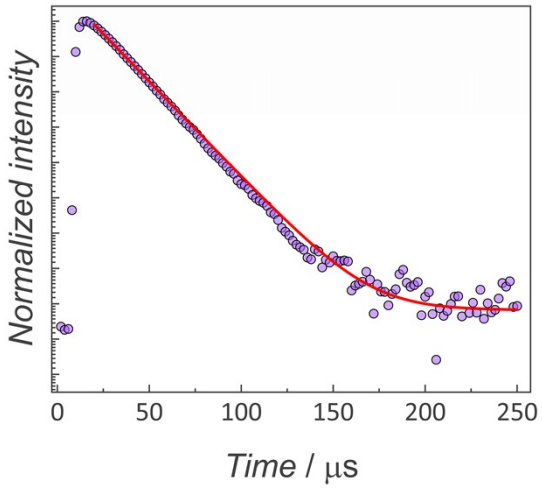

Fig.S6. Emission decay curves (9 K) obtained from microcrystalline [Dy(acac)$_3$bpm] (**1**) excited at 330 nm and monitoring the emission at 575 nm. The solid lines correspond to the data best fit (R^2>0.99), using a monoexponential function.

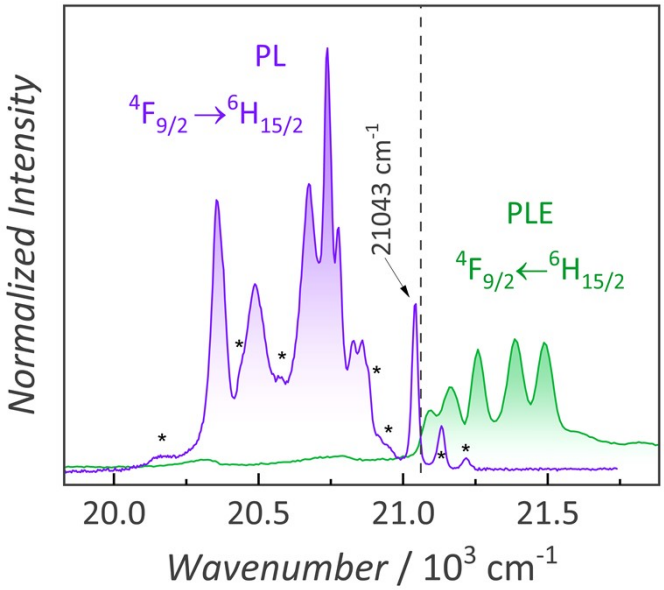

Fig. S7. High-resolution excitation (PLE, λ_{em} = 575 nm) and emission (PL, λ_{exc} = 330 nm) spectra at 9 K representing the $^4F_{9/2} \leftarrow {}^6H_{15/2}$ and $^4F_{9/2} \rightarrow {}^6H_{15/2}$ transitions, respectively, used to estimate the energy diagram represented in Fig. 2a. The partial energy level diagram was determined as follows: As a consequence of the CF splitting, (J+1/2) M_J (KDs) components are expected for each $^{2S+1}L_J$ level. In the case of the $^6H_{15/2}$ ground level, 8 M_J components are expected in the emission spectrum (assuming that only the first M_J sublevel arising from the $^4F_{9/2}$ emitting level is populated). Yet, additional signals are observed (denoted with* and named as "hot bands"), suggesting that the two lower-energy M_J of the emitting $^4F_{9/2}$ level are populated. Due to the low temperature and according to the Boltzmann distribution, the components arising from the upper energy M_J excited level should render lower intensity emission bands. In light of this guidance, an energetic difference between the M_J sublevels of the ground and emitting levels was obtained, Table S6.

Table S6. Relative energies of the Stark sublevels (M_J or KD) of the $^6H_{15/2}$ and $^6H_{13/2}$ Dy^{III} levels obtained from the experimental luminescence data of [Dy(acac)$_3$bpm] (**1**). ΔE is the energy difference between the KD and the other closest lower energy KD.

	Relative energy / cm^{-1}	ΔE / cm^{-1}
Dy^{III} $^6H_{15/2}$ level		
KD1	0	0
KD2	187	187
KD3	216	29
KD4	269	53
KD5	305	36
KD6	369	64
KD7	557	188
KD8	687	130
Dy^{III} $^4F_{9/2}$ level		
KD1	21087	0
KD2	21161	74
KD3	21259	98
KD4	21385	126
KD5	21486	101

Supplementary note S5 - Additional magnetic data

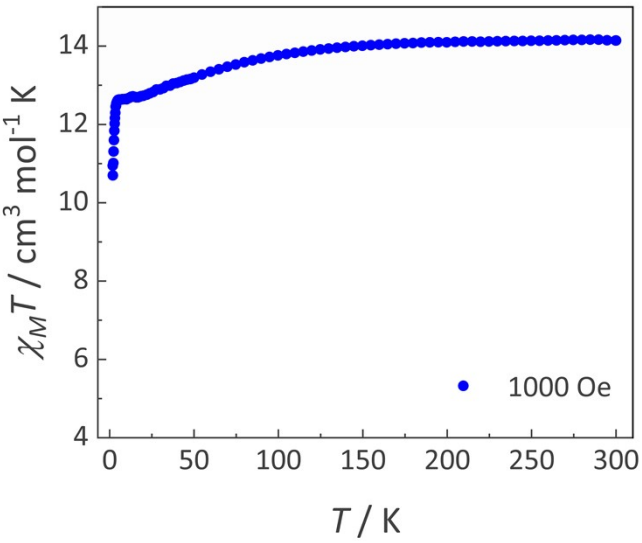

Fig. S8. Temperature (T) dependence plot of the molar magnetic susceptibility ($\chi_M T$) under an applied field of 1000 Oe, from 1.8 K to 300 K, for [Dy(acac)$_3$bpm] (**1**). The $\chi_M T$ product reaches a value of 14.14 cm^3 mol^{-1} K at 300 K, which is in agreement with the theoretical free-ion value for Dy^{III} ($^6H_{15/2}$, g = 4/3, C = 14.17 cm^3 mol^{-1} K).

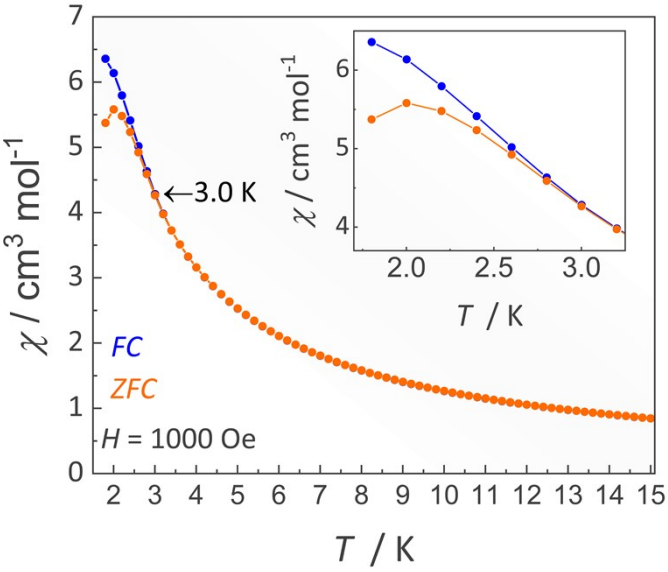

Fig. S9. Zero-field-cooled/field-cooled (ZFC/FC) measurements (1 K min^{-1}) of [Dy(acac)$_3$bpm] (**1**).

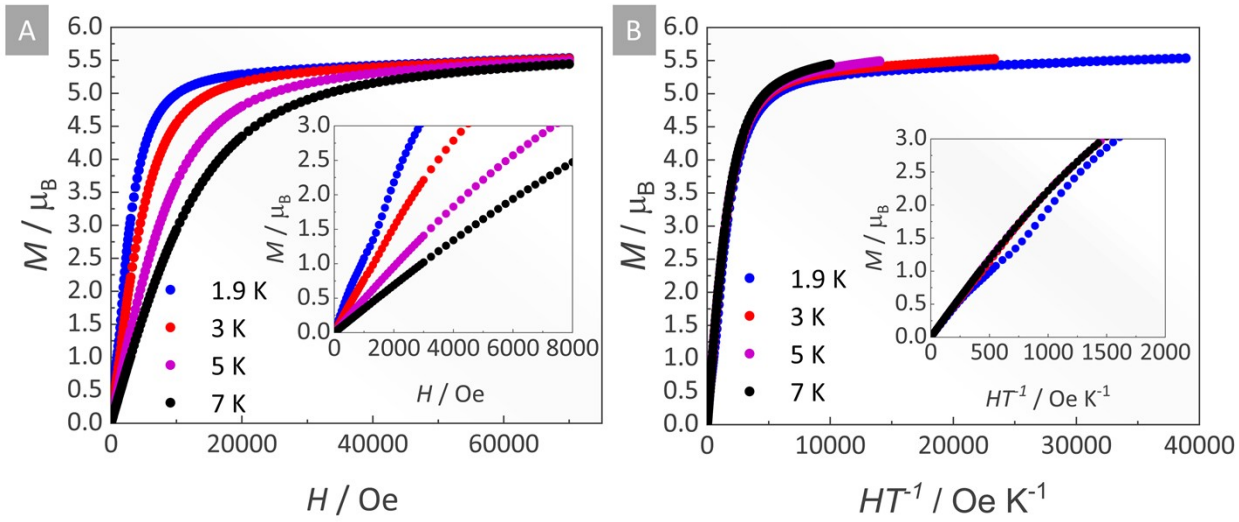

Fig. S10. Field (*H*) dependence plot of the (a) magnetization (*M*) and (b) the reduced magnetization (HT^{-1}) at different temperatures (1.9, 3, 5, or 7 K) of [Dy(acac)$_3$bpm] (**1**). The inserts in the figures represent the magnification of the curves up to (a) *H* = 8000 Oe and (b) HT^{-1} = 40000 Oe K^{-1}. In the magnetization (*M vs. H*) and reduced magnetization (M *vs.* HT^{-1}) plots, the magnetization increases as temperature decreases and the magnetic field increases, whose maximum is achieved at 5.53 μB (1.9 K), 5.52 μB (3.0 K), 5.49 μB (5.0 K), and 5.44 μB (7 K). In (a), after 35 kOe, saturation starts to be observed for the isotemperature lines measured at 1.9 and 3 K, and after 60 kOe, for the ones at 5 and 7 K.

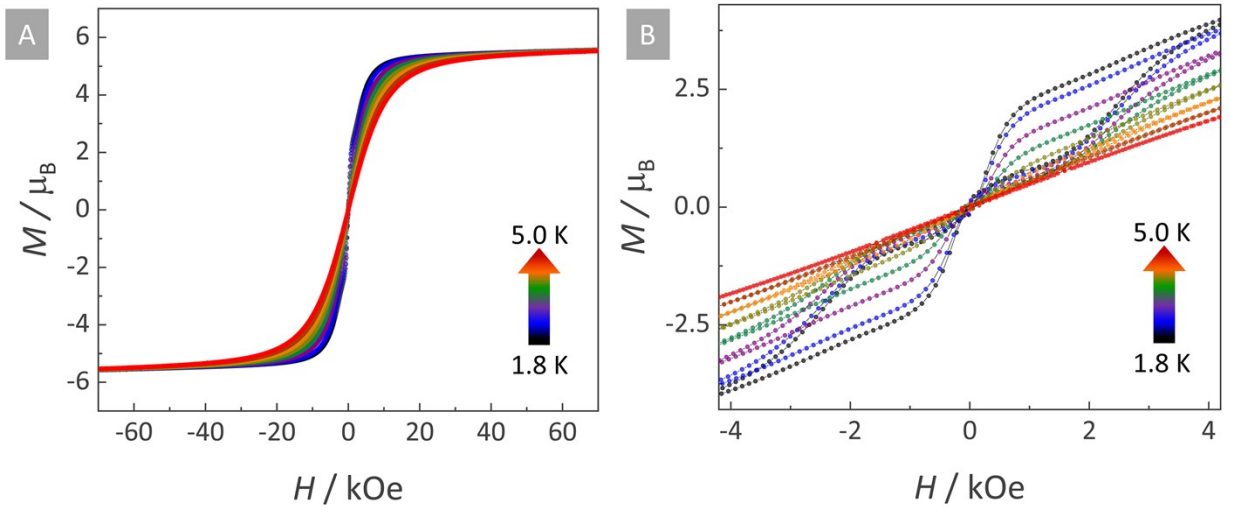

Fig. S11. Magnetic hysteresis plot (magnetization *versus* applied field) at 1.8, 2.0, 2.5, 3.0, 3.5, 4.0, 4.5, and 5.0 K (25 Oe s^{-1}) of [Dy(acac)$_3$bpm] (**1**).

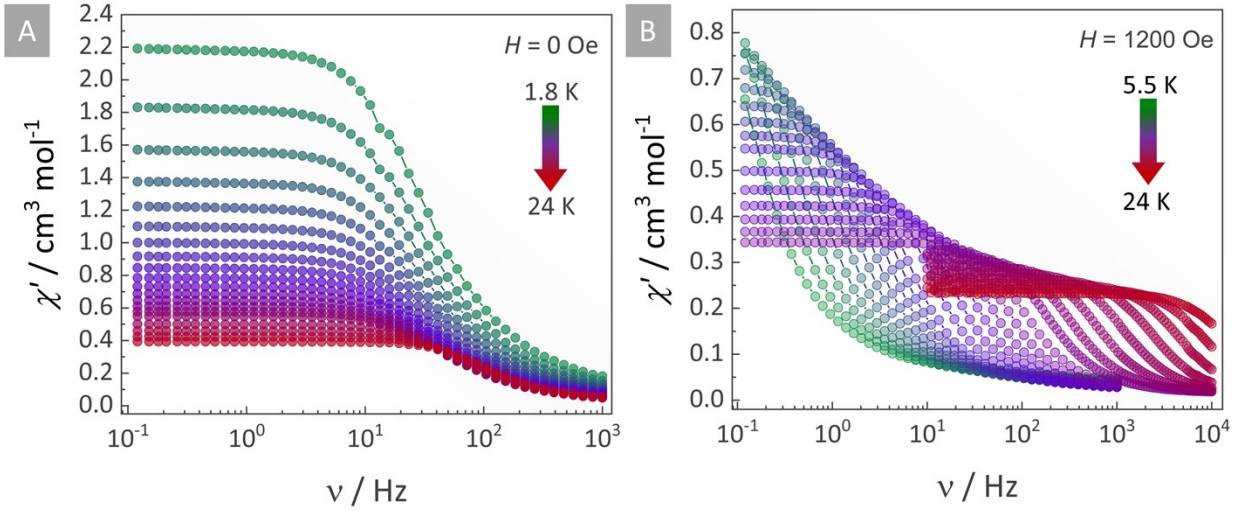

Fig. S12. Frequency (ν) dependence of the in-phase molar magnetic susceptibilities (χ') at (a) 0 Oe and (b) 1200 Oe for [Dy(acac)$_3$bpm] (**1**).

$$\chi'' = \frac{(\chi_t - \chi_s)(2\pi\nu t)^{(1-\alpha)}\cos\left(\frac{\alpha\pi}{2}\right)}{\left[1 + (2(2\pi\nu t)^{(1-\alpha)})\sin\left(\frac{\alpha\pi}{2}\right) + (2\pi\nu t)^{2(1-\alpha)}\right]} \quad (S1)$$

$$\chi'' = \frac{(\chi_t - \chi_s)(2\pi\nu t)^{(1-\alpha)}\cos\left(\frac{\alpha\pi}{2}\right)}{\left[1 + (2(2\pi\nu t)^{(1-\alpha)})\sin\left(\frac{\alpha\pi}{2}\right) + (2\pi\nu t)^{2(1-\alpha)}\right]} + \frac{(\chi_{tg} - \chi_{sg})(2\pi\nu t_g)^{(1-\alpha_g)}\cos\left(\frac{\alpha_g\pi}{2}\right)}{\left[1 + \left(2(2\pi\nu t_g)^{(1-\alpha)}\right)\sin\left(\frac{\alpha_g\pi}{2}\right) + (2\pi\nu t_g)^{2(1-\alpha_g)}\right]} \quad (S2)$$

Table S7. Best-fit parameters (χ_s, χ_t, α, τ) to the single Debye model (eqn S1) for the frequency (ν) dependence of the out-of-phase magnetic susceptibility (χ'') as a function of the temperature (T) collected in the absence of an external magnetic field for [Dy(acac)$_3$bpm] (**1**).

H / Oe	χ_s / cm^3 mol^{-1}	χ_t / cm^3 mol^{-1}	α	τ / s
1.8	0.02943	2.87598	0.17417	0.00466
2.0	0.1994	2.76593	0.17456	0.00464
2.5	0.00898	2.07706	0.17318	0.00459
3.0	0.00199	1.7292	0.17158	0.00456
3.5	0.0014	1.48746	0.17313	0.00451
4.0	0.00289	1.29954	0.17452	0.00446
4.5	0.00343	1.15564	0.17489	0.00442
5.0	0.00678	1.04235	0.1722	0.00438
5.5	0.05379	0.99339	0.17343	0.00434
6.0	0.0272	0.88846	0.17281	0.00426
6.5	0.03535	0.83171	0.16977	0.00417
7.0	0.00345	0.75001	0.14089	0.20833
7.5	3.98616E-4	0.69077	0.16284	0.0039
8.0	0.01079	0.65629	0.16273	0.00375
8.5	2.55771E-4	0.60795	0.15922	0.00359
9	0.0075	0.58039	0.15412	0.00339
9.5	0.00121	0.54354	0.14774	0.00317
10	7.83328E-4	0.51455	0.14029	0.00293
11	0.00402	0.47221	0.12523	0.00248
12	1.94696E-4	0.42731	0.11205	0.00203
13	2.65739E-5	0.39357	0.0978	0.00163
14	8.08572E-5	0.36407	0.08512	0.00127
15	8.26795E-5	0.33781	0.07285	9.71354E-4
16	8.97687E-4	0.31521	0.05777	7.12603E-4
17	6.03627E-4	0.31159	0.09655	4.59744E-4
18	6.31862E-4	0.29184	0.07959	2.75853E-4
19	0.00205	0.28101	0.07056	1.8031E-4
20	0.00442	0.27143	0.05749	1.05201E-4
21	2.71467E-4	0.25442	0.04711	5.99662E-5
22	1.11764E-4	0.24155	0.04802	3.35346E-5
23	0.00172	0.22827	0.04547	1.8931E-5
24	3.40554E-4	0.20998	0.04505	1.10152E-5

Table S8. Summary of the fit parameters of the temperature (T) dependent relaxation time of the magnetization (τ^{-1}) at H = 0 Oe and 1200 Oe obtained from eqn S3.

Mechanism	Parameter	0 Oe	1200 Oe
Orbach	U_{eff}	309 K (215 cm^{-1})	345 K (239 cm^{-1})
	τ_0	3.2 10^{-11} s	6.1 10^{-12} s
Raman	C	1.4 10^{-3} s^{-1} K^{-n}	3.1 10^{-5} s^{-1} K^{-n}
	n	4.9	6.1
QTM	τ_{QTM}	4.5 10^{-3} s	-

$$\tau^{-1} = \tau_{QTM}^{-1} + \tau_0^{-1} exp\left(-\frac{U_{eff}}{K_B T}\right) + CT^n \quad (S3)$$

In eqn S3, the first term represents the quantum tunnelling of magnetisation (QTM) contribution, U_{eff} and τ_0 represent the effective barrier and the pre-exponential factor obtained from the Orbach contribution, C and n are the parameters obtained from the Raman process, and τ_{QTM} is the time constant of the QTM contribution

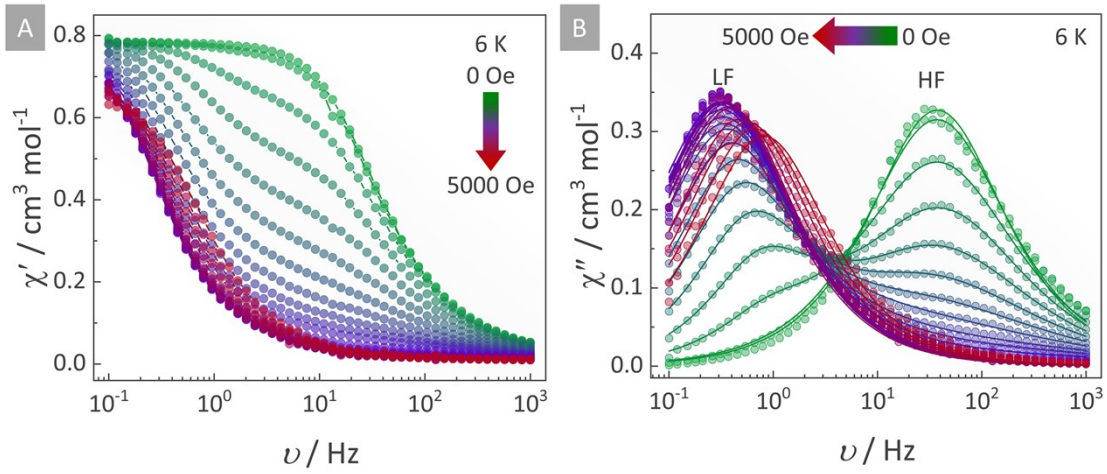

Fig. S13. Frequency (ν) dependence of the (a) in-phase (χ') and (b) out-of-phase (χ'') magnetic susceptibility as a function of the applied field (H, from 0 Oe to 5000 Oe) at 6 K for [Dy(acac)$_3$bpm] (**1**). The solid lines represent the best fit to the Debye model, where the sum of two Debye equations was necessary to fit the two independent processes present within the field range of 200-1000. The fit parameters are provided in Table S9.

Table S9. Best-fit parameters (χ_s, χ_t, α, τ) to the generalized Debye model for the frequency (ν) dependence of the out-of-phase magnetic susceptibility (χ'') as a function of applied field (H) at 6 K. Two separate Debye equations were used to account for the two independent processes present within the field range of 200-1000 Oe.

H / Oe	χ_s / cm³ mol⁻¹	χ_t / cm³ mol⁻¹	α	τ^{-1} / s⁻¹	χ_s / cm³ mol⁻¹	χ_t / cm³ mol⁻¹	α	τ / s
0	0.0272	0.88846	0.17281	0.00426				
100	0.0074	0.87511	0.20049	0.00428				
200	0.00107	0.7762	0.25171	0.00418	0.00644	0.10553	0.01809	0.17405
300	0.01607	0.64218	0.28606	0.00391	0.01062	0.2627	0.03838	0.20312
400	0.00293	0.50443	0.32958	0.00398	0.00654	0.39321	0.07458	0.25639
500	0.00278	0.41752	0.39382	0.00459	0.06234	0.54578	0.08842	0.31336
600	0.01707	0.36917	0.46558	0.00597	0.00114	0.56035	0.1002	0.36725
700	0.00521	0.33693	0.55293	0.01141	0.02911	0.63443	0.1127	0.42032
800	0.00121	0.31807	0.65562	0.03464	0.03095	0.69631	0.139	0.45226
900	0.02455	0.30707	0.69129	0.07042	5.81326E-4	0.71399	0.1567	0.47656
1000	0.01495	0.23068	0.74093	0.13663	0.03009	0.81691	0.1768	0.48247
1200					0.00255	0.91131	0.20552	0.51083
1400					0.00999	0.91686	0.19162	0.51416
1600					0.00184	0.90067	0.18025	0.51073
1800					0.01242	0.89433	0.17024	0.48843
2000					0.00103	0.87626	0.16311	0.48026
2200					0.00181	0.87419	0.16172	0.46811
2400					0.00826	0.87281	0.16049	0.45241
2600					0.01698	0.87031	0.15921	0.42856
2800					0.00151	0.83969	0.15118	0.40388
3000					0.09628	0.81938	0.15025	0.38664

3500		0.01023	0.80942	0.14874	0.33477
4000		0.0043	0.79245	0.14776	0.28139
4500		0.01059	0.77514	0.14633	0.23636
5000		0.01058	0.75134	0.14582	0.19508

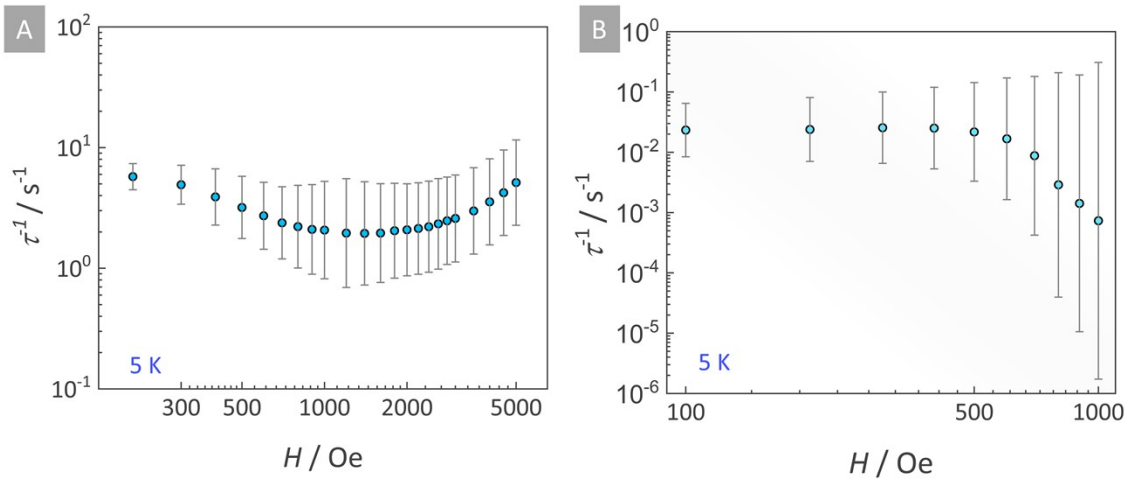

Fig. S14. Field (*H*) dependence of the relaxation rate of magnetization (τ^{-1}) at 6 K for the (a) lower frequency (LF) and (b) higher frequency (HF) processes observed in Fig. S13b. The uncertainties of relaxation time parameter were calculated accordingly to D. Reta, N. F. Chilton.[24]

Table S10. Best-fit parameters (χ_s, χ_t, α, τ) to the generalized single Debye model (eqn S1) for the frequency (ν) dependence of the out-of-phase magnetic susceptibility (χ'') as a function of the temperature (T). Data was collected under an external magnetic field of 1200 Oe.

***H* / Oe**	**χ_s / cm^3 mol^{-1}**	**χ_t / cm^3 mol^{-1}**	**α**	**τ / s**
5.5	0.0289	1.24951	0.27827	1.58031
6.0	0.00255	0.91131	0.20552	0.51083
6.5	0.00142	0.82756	0.16783	0.34517
7.0	0.00345	0.75001	0.14089	0.20833
7.5	0.00679	0.69609	0.12516	0.1342
8.0	5.60247E-4	0.64444	0.11583	0.08994
8.5	0.00556	0.61016	0.10769	0.06226
9	0.00122	0.57173	0.10141	0.0443
9.5	5.48517E-4	0.54112	0.09683	0.03222
10	7.50921E-4	0.51477	0.09291	0.02386
11	1.28532E-4	0.46873	0.08731	0.01386
12	3.24425E-4	0.43048	0.08108	0.00843
13	0.00106	0.39866	0.07582	0.00536
14	5.09598E-4	0.3696	0.07372	0.00347
15	1.59854E-5	0.34312	0.06989	0.00222
16	3.63919E-4	0.32065	0.06149	0.0014
17	0.00141	0.31888	0.09834	8.09319E-4
18	0.00448	0.30369	0.0944	4.59778E-4
19	1.99651E-4	0.28213	0.08547	2.47255E-4
20	0.00329	0.26983	0.07344	1.27771E-4
21	0.00538	0.25774	0.06012	6.5967E-5

22	0.00168	0.24228	0.05458	3.45753E-5
23	6.61225E-5	0.22821	0.04424	1.86935E-5
24	0.0016	0.22401	0.05211	1.00404E-5

Supplementary note S6 – Luminescence thermometry

The relative thermal sensitivity of the complex was calculated from eqn S4, where Δ is the thermometric parameter and T is the temperature. The temperature uncertainty (δT) is calculated by eqn S5 and eqn S6, where $\delta I/I$ is the relative uncertainty in the integrated area.[25] δI was calculated from the signal-to-noise ratio for each normalized spectrum measured within the 555 – 595 nm spectral range, which was close to 0.015 for all of them. Thus, eqn S6 can be reduced to $\delta I/I = 0.015$ for all spectra considering the normalized spectra since $I_{max} = 1$.

$$S_r = \frac{1}{\Delta}\left|\frac{d\Delta}{dT}\right| \quad (S4)$$

$$\delta T = \frac{1}{S_r}\frac{\delta\Delta}{\Delta} \quad (S5)$$

$$\frac{\delta\Delta}{\Delta} = \sqrt{\left(\frac{\delta I_1}{I_1}\right)^2 + \left(\frac{\delta I_2}{I_2}\right)^2} = \sqrt{2}\frac{\delta I}{I} \quad (S6)$$

Table S11. Fitting parameter obtained using a logistic function (eqn S7) to describes the dependence of the thermometric parameter on temperature for [Dy(acac)$_3$bpm] (**1**).

Parameter	Value
A_1	*0.4396*
A_2	*6.919*
T_0 / K	*221.4*
p	*2.370*

$$\Delta = A_2 + \frac{A_1 - A_2}{1 + \left(\frac{T}{T_0}\right)^p} \quad (S7)$$

Supplementary references

[1] P-P. Cen, S. Zhang, X-Y. Liu, W-M. Song, Y-Q. Zhang, G. Xie, S-P. Chen, *Inorg. Chem.,* 2017, **56**, 3644.

[2] E.V. Gorshkov, D. V. Korchagin , E. A. Yureva, G. V. Shilov, M. V. Zhidkov, A. I. Dmitriev, N. N. Efimov, A. V. Palii, S. M. Aldoshin, *Magnetochemistry,* 2022, **8**, 151.

[3] M. Kong, X. Feng, J. Li, Z-B. Hu, J. Wang, X-J. Song, Z-Y. Jing, Y-Q. Zhang, Y. *Dalton Trans.,* 2020, **49**, 14931.

[4] J. Xi, X. Ma, P. Cen, Y. Wu, Y-Q. Zhang, Y. Guo, J. Yang, L. Chen, X. Liu, *Dalton Trans.,* 2021, **50**, 2102.

[5] G-J. Chen, Y-N. Guo, J-L. Tian, J. Tang, W. Gu, X. Liu, S-P. Yan, P. Cheng, D-Z. Liao, *Chem. Eur. J.*, 2012, **18**, 2484.

[6] Y-Z. Tong, C. Gao, Q-L. Wang, B-W. Wang, S. Gao, P. Cheng, D-Z. Liao, *Dalton Trans.*, 2015, **44**, 9020.

[7] M. Guo, J. Wu, O. Cador, J. Lu, B. Yin, B. L. Guennic, J. Tang, *Inorg. Chem.*, 2018, **57**, 4534.

[8] G-J. Chen, C-Y. Gao, J-L Tian, J. Tang, W. Gu, X. Liu, S-P. Yan, D-Z. Liao, P. Cheng, *Dalton Trans.*, 2011, **40**, 5579.

[9] G-J. Chen, Y. Zhou, G-X. Jin, Y-B. Dong, *Dalton Trans.*, 2014, **43**, 16659.

[10] R. Marin, D. A. Galico, R. Gayfullina, J. O. Moilanen, L. D. Carlos, D. Jaque, M. Murugesu, *J. Mater. Chem. C*, 2022, **10**, 13946.

[11] R. A. S. Ferreira, E. Mamontova, A. M. P. Botas, M. Shestakov, J. Vanacken, V. Moshchalkov, Y. Guari, L. F. Chibotaru, D. Luneau, P. S. André, J. Larionova, J. Long, L. D. Carlos, *Adv.Optical Mater.*, 2021, **9**, 2101495.

[12] K. Kumar, O. Stefanczyk, S. Chorazy, K. Nakabayashi, S. Ohkosh, *Adv.Optical Mater.*, 2022, **10**, 2201675.

[13] V. Tangoulis, V. Nastopoulos, N. Panagiotou, A. Tasiopoulos, G. Itskos, M. Athanasiou, E. Moreno-Pineda, W. Wernsdorfer, M. Schulze and O. Malina, *Inorg. Chem.*, 2022, **61**, 2546.

[14] J. Corredoira-Vázquez, C. González-Barreira, M. Fondo, A. M. García-Deibe, J. Sanmartín-Matalobos, M. A. Hernández-Rodríguez, L. D. Carlos, *Dalton Trans.*, 2022, **51**, 15593.

[15] D. Errulat, R. Marin, D. A. Gálico, K. L. M. Harriman, A. Pialat, B. Gabidullin, F. Iikawa, O. D. D. Couto-Jr., J. O. Moilanen, E. Hemmer, F. A. Sigoli, M. Murugesu *ACS Cent. Sci.*, 2019, **5**, 1187.

[16] A. A. Kitos, D. A. Galico, N. Mavragani, R. Castaneda, J. O. Moilanen, J. L. Brusso, M. Murugesu, *Chem. Commun.*, 2021, **57**, 7818.

[17] K. Karachousos-Spiliotakopoulos, V. Tangoulis, N. Panagiotou, A. Tasiopoulos, V. Nastopoulos, E. Moreno-Pineda, W. Wernsdorfer, M. Schulze, A. M. P. Botas, L. D. Carlos, *Inorg. Chem.*, 2022, **61**, 46, 18629.

[18] P. F. H. Schwab, F. Fleischer, J. Michl, *J. Org. Chem*., 2002, **67**, 2, 443.

[19] O. V. Dolomanov, L. J. Bourhis, R. J. Gildea, J. A. K. Howard, H. Puschmann, *J. Appl. Cryst.*, 2009, **42**, 339.

[20] G. M. Sheldrick, *Acta Cryst.*, 2015, **A71**, 3.

[21] G. M. Sheldrick, *Acta Cryst.*, 2015, **C71**, 3.

[22] M. Pinsky, D. Avnir, Continuous Symmetry Measures. 5. The Classical Polyhedra. *Inorg. Chem.*, 1998, **37**, 5575.

[23] N. F. Chilton, D. Collison, E. J. L. McInnes, R. E. P. Winpenny, A. Soncini, *Nat. Commun.*, 2013, **4**, 2551.

[24] D. Reta, N. F. Chilton, *Phys. Chem. Chem. Phys.*, 2019, **21**, 23567.

[25] Brites, C. D. S.; Millán, A.; Carlos, L. D. Lanthanides in Luminescent Thermometry. In: Handbook on the Physics and Chemistry of Rare Earths; Elsevier, 2016; pp 339-427.